Radiocarbon, Vol 59, Nr 1, 2017, p 231–249 DOI:10.1017/RDC.2017.7

ACCURATE RADIOCARBON DATING OF ARCHAEOLOGICAL ASH USING PYROGENIC ARAGONITE

Michael B Toffolo[1*] • Lior Regev[2] • Eugenia Mintz[2] • Kristin M Poduska[3] • Ruth Shahack-Gross[4] • Christoph Berthold[5] • Christopher E Miller[1,6] • Elisabetta Boaretto[2*]

[1]Institut für Naturwissenschaftliche Archäologie, Eberhard-Karls-Universität Tübingen, Tübingen 72070, Germany.
[2]Max Planck-Weizmann Center for Integrative Archaeology and Anthropology, D-REAMS Radiocarbon Dating Laboratory, Weizmann Institute of Science, Rehovot 76100, Israel.
[3]Department of Physics and Physical Oceanography, Memorial University Newfoundland, St. John's NL A1B 3X7, Canada.
[4]Department of Maritime Civilizations, University of Haifa, Haifa 3498838, Israel.
[5]Competence Center Archaeometry – Baden-Württemberg (CCA-BW), Angewandte Mineralogie, Fachbereich Geowissenschaften, Eberhard-Karls-Universität Tübingen, Tübingen 72074, Germany.
[6]Senckenberg Centre for Human Evolution and Palaeoenvironment, Eberhard-Karls-Universität Tübingen, Tübingen 72070, Germany.

ABSTRACT. Obtaining accurate age determinations from minerals in archaeological ash is a major unsolved issue in radiocarbon (^{14}C) dating. This is because the original ^{14}C content of calcite, the main component of ash, is altered by isotopic exchange. Pyrogenic aragonite, another mineral phase recently discovered in ash, might preserve its ^{14}C signature through time. Using a new method based on density separation and step combustion, we were able to isolate and date aragonitic ash from an archaeological destruction horizon of known age. Here we show that the ^{14}C age of aragonite matches the age of the destruction horizon. Our results demonstrate that pyrogenic aragonite is a short-lived material suitable for ^{14}C dating and directly related to human activities involving the use of fire, thus bearing major implications for the establishment of absolute chronologies for the past 50,000 yr.

KEYWORDS: ash, aragonite, calcite, diagenesis, density separation.

INTRODUCTION

Ash is the powdery residue left after the combustion of organic materials, and one of the most common components of sediments at archaeological sites (Weiner 2010). Being the most direct byproduct of combustion, ash is an important indicator of past human activities involving the use of fire (Weiner 2010; Wadley et al. 2011). Therefore, the identification of combustion features is crucial in understanding human evolution, behavior, and practices (Wrangham 2009; Roebroeks and Villa 2011; Gowlett and Wrangham 2013). The identification is achieved by studying the microscopic archaeological record using different analytical methods that characterize the mineral and organic components present in ash (Weiner 2010; Berna et al. 2012; Shahack-Gross et al. 2014; Walker et al. 2016). Often, these components are organized in distinct layers of sediment, which are the result of single or multiple firing episodes, and thus represent well-defined, short-lived events within a stratigraphic sequence that are suitable for radiocarbon (^{14}C) dating (e.g. Adler et al. 2008; Kuhn et al. 2009; Rebollo et al. 2011; Regev et al. 2014; Asscher et al. 2015a, 2015b). Considering the widespread occurrence of ash deposits in archaeological settings across the globe, it appears clear that obtaining accurate ages from these features is of major importance for the establishment of absolute chronologies, and thus for sequencing events along the human career.

To date, ^{14}C measurements of ash have always been performed on the organic fraction, namely charcoal and charred seeds that may survive when the combustion process is incomplete (Taylor and Bar-Yosef 2014). However, charcoal suffers from the "old wood" effect (Bowman 1990), whereas charred seeds might be unrelated to the depositional context, especially if they do not occur in sealed clusters (Toffolo et al. 2012; Asscher et al. 2015a). Charred materials

*Corresponding authors. Email: elisabetta.boaretto@weizmann.ac.il; michael.toffolo@ifu.uni-tuebingen.de.

in general are often not preserved in ash due to post-depositional alterations (Cohen-Ofri et al. 2006; Rebollo et al. 2008). Thus, in many cases only the mineral components are left. Among these, the most abundant is calcium carbonate ($CaCO_3$) in the form of calcite, which is the product of thermal decomposition of biogenic calcium oxalate ($C_2CaO_4{\cdot}H_2O$) produced by plants (Frost and Weier 2004; Franceschi and Nakata 2005). This calcite phase contains ^{14}C, which in principle derives from atmospheric CO_2 sequestered by plants during photosynthesis, and therefore could be used for accurate dating. However, a previous study pointed out that the isotopic signature of ash calcite is different compared to the plant cellulose one, thus hampering a proper age assessment (Regev et al. 2011). In addition, CO exchange between calcium oxalate and the atmosphere during burning may alter the initial ^{14}C content (Price et al. 1980; Regev et al. 2011). If the firing temperature exceeds 600°C, the calcite derived from calcium oxalate turns into calcium oxide (CaO) (Frost and Weier 2004). This mineral phase is unstable at ambient temperature, and when the firing stops, it turns again into calcite by reacting with humidity and CO_2 in the atmosphere (Boynton 1980). This high-temperature calcite bears the ^{14}C signature of the atmosphere at the time it nucleates, and therefore could provide accurate ^{14}C dates. In practice, this is not the case because ash always undergoes diagenetic processes that partially or totally alter its original isotopic composition (Koumouzelis et al. 2001; Weiner et al. 2002). Recently, we reported that another polymorph of $CaCO_3$, aragonite, forms together with calcite upon carbonation of CaO in experimental and archaeological high-temperature ash (Toffolo and Boaretto 2014). This pyrogenic aragonite phase is an ideal material for ^{14}C dating. It occurs in archaeological combustion features, it represents the time of ash formation, and since it is susceptible to post-depositional chemical alterations, its presence indicates pristine conditions of preservation, which might include the original ^{14}C signature. Here we show that by carefully isolating pyrogenic aragonite from a destruction horizon of known age at the site of Tel Megiddo, Israel (Figure 1A), it was possible to measure its ^{14}C content and obtain an accurate age determination.

MATERIALS AND METHODS

Archaeological Context and Sampling

Tel Megiddo, located in northern Israel (Figure 1A), is one of the most important archaeological sites in the Levant, featuring an uninterrupted stratigraphic sequence from the Neolithic to the Persian period (Finkelstein et al. 2000, 2006, 2013). A recent ^{14}C dating program, based on clusters of charred olive pits collected from secure depositional contexts, established a high-resolution chronological sequence spanning the period from the Middle Bronze Age III through to the Iron Age IIA (Toffolo et al. 2014). Within this period, three destruction events characterized by large amounts of in-situ crushed ceramics and burnt debris provided important pegs for both the relative and absolute chronologies. One of these destruction events marks the end of the Iron Age I material culture, which represents the collapse of the late Canaanite city-state (Finkelstein et al. 2006). This destruction event has been unearthed in different excavation areas and dated to the range 2920–2760 BP (69.59–70.93 pMC) (Toffolo et al. 2014). During the 2014 excavation season, preliminary on-site analysis carried out by one of us (RSG) revealed the presence of aragonite within Level K-4, which includes the Iron Age I destruction horizon in Area K. In the NW section of the Area K trench, Level K-4 features three layers belonging to the destruction horizon (Figures 1B and 1C). A black layer rich in charred material covered by potsherds underlies a thin white ashy layer rich in aragonite, which in turn is covered by a massive burnt mudbrick collapse. This locality was selected for detailed sampling. Bulk sediment samples were collected from each layer and

https://doi.org/10.1017/RDC.2017.7 Published online by Cambridge University Press

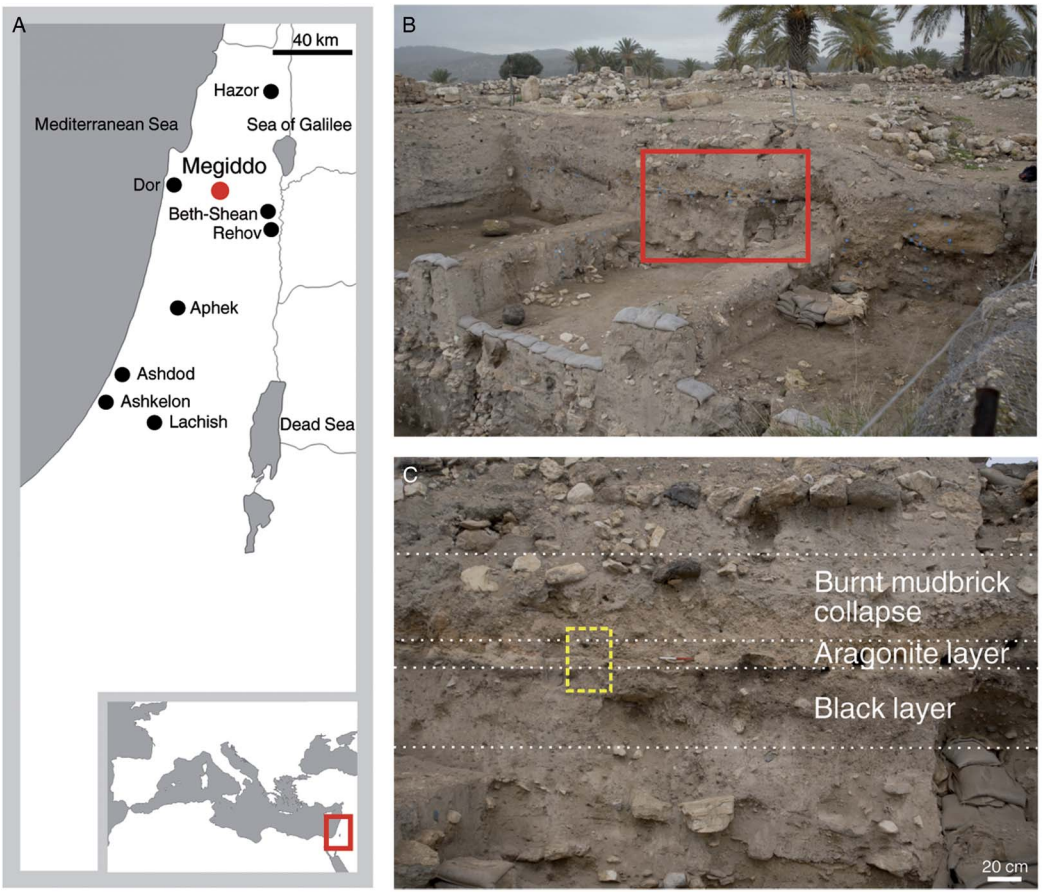

Figure 1 Site location and archaeological context. A: map showing the location of Tel Megiddo and other major Iron Age sites in southern Levant. B: view of the NW trench section of Area K. The rectangle marks the sampling locality. C: view of the portion of the destruction horizon highlighted in B, showing the stratigraphic sequence belonging to Level K-4. The dashed rectangle marks the position of the micromorphology block and the sample dated with ^{14}C.

stored in plastic vials and bags, which provided enough material for all the laboratory analyses. Two charred olive pits found together within the black layer were collected with their sediment matrix and stored in aluminum foil for ^{14}C dating. Chalk from the local bedrock was used as a reference for stable isotopes and thermogravimetric analyses.

Experimental Samples

An experimental ash rich in aragonite was used as a reference for scanning electron microscope (SEM) analysis and ^{14}C dating. This material was obtained by heating *Glycymeris insubrica* shells to 900°C for 12 hr in air atmosphere using an electric muffle oven. The resulting quicklime (CaO) was quenched to room temperature in ambient air (Toffolo and Boaretto 2014). At the time of this study, the ash was 3 yr old and composed of a mixture of aragonite (dominant), calcite, and portlandite [$Ca(OH)_2$]. A crystal of pure geogenic aragonite from a Triassic formation in Loma Badá (Spain), purchased from Mineralogical Research Company (San Jose, California, USA), was used as blank for the density separation method and ^{14}C dating.

https://doi.org/10.1017/RDC.2017.7 Published online by Cambridge University Press

Fourier Transform Infrared Spectrometry (FTIR)

A few milligrams of sediment were homogenized and powdered in an agate mortar and pestle. About 0.1 mg was left in the mortar and mixed with approximately 0.5 mg of KBr (FTIR grade, Sigma-Aldrich) and pressed into a 7-mm pellet using a hydraulic press (Specac) or a hand press (PIKE Technologies). Infrared spectra were obtained at 4 cm^{-1} resolution in 32 scans within the 4000–400 cm^{-1} spectral range using a Thermo Scientific Nicolet 380 spectrometer (for archaeological sediments and density separation fractions analyzed at the Weizmann Institute of Science) and an Agilent Technologies Cary 660 spectrometer (for fractions obtained from density separation analyzed at Eberhard-Karls-Universität Tübingen). Phase identification was performed using OMNIC v. 9, standard literature (Farmer 1974; van der Marel and Beutelspacher 1976), and the reference collection of FTIR spectra of standard materials provided by the Kimmel Center for Archaeological Science, Weizmann Institute of Science (http://www.weizmann.ac.il/kimmel-arch/infrared-spectra-library). The crystallinity index, or splitting factor, of hydroxylapatite was calculated using an established method (Weiner and Bar-Yosef 1990).

Phytolith Analysis

Phytolith assemblages were obtained using the rapid extraction method (Katz et al. 2010). The identification of different morphotypes was carried out following the standard literature and a reference collection of archaeological and modern samples (Twiss et al. 1969; Mulholland and Rapp 1992; Madella et al. 2005; Albert et al. 2016). Phytoliths were studied using a Zeiss Axio Scope AX10 petrographic microscope at 200× and 400× magnifications.

Archaeological Micromorphology

An intact block of sediment was carved from the NW section of Area K, air-dried for several weeks and finally oven-dried at 40°C for 3 days. The sample was then embedded in a mixture of polyester resin (Elgad, Israel) and acetone (ratio 7:3), with the addition of 10 mL of MEKP catalyst per 1 L of mixture. Once solid, the block was cured in an oven at 50°C for three days and then sliced with a rock saw to obtain 55 × 75 mm chips, which were shipped to Arizona Quality Thin Sections (Tucson, Arizona, USA) for thin section preparation. All the thin sections were polished to a thickness of 30 µm. Micromorphological analyses were carried out using a Nikon Eclipse 50iPOL petrographic microscope at different magnifications (20×, 100×, 200×, 400×), following the standard literature (Courty et al. 1989; Stoops et al. 2010).

X-Ray Diffraction (XRD)

Bulk and sieved (<50 µm) ash samples were analyzed using a D8 Discover GADDS micro-diffractometer (µ-XRD^2) equipped with a cobalt-sealed tube running at 30kV/30mA, a HOPG primary monochromator, a 500 µm monocapillary optic with a 300 µm exit pinhole, and a large 2D detector (VÅNTEC-500) covering 40°2θ and χ. Samples were prepared on a low background silicon single-crystal wafer, used as sample holder. Phase identification was performed using EVA v. 10 and DIFFRAC Plus Release 2004, and a PDF database from the International Centre for Diffraction Data (ICDD). Crystalline phases were quantified using the Rietveld software package Siroquant v. 3.0.

Raman Micro-Spectrometry (µ-Raman)

Sieved ash samples (<50 µm) were analyzed using a Renishaw inVia Raman microscope. Analyses were carried out using a 532 nm laser with 1800 lines/mm grating at 50% power. Each measurement consists of five accumulations over 5 s at 50× magnification. Phase identification

https://doi.org/10.1017/RDC.2017.7 Published online by Cambridge University Press

was performed using reference materials of the Angewandte Mineralogie Department at Eberhard-Karls- Universität Tübingen (validated by XRD), and the RRUFF database (http://rruff.info).

Scanning Electron Microscopy (SEM)

Sediment samples were placed on carbon tape and coated with a Au-Pd sputter coater (Edwards S150). Samples were examined with a high-resolution Zeiss Leo Supra 55VP field emission scanning electron microscope. Analyses were performed between 2 and 5 kV at various working distances using a secondary electron detector.

Stable Isotopes Analysis

The carbon and oxygen isotope compositions of chalk and aragonite-rich ash were determined using a GasBench II device connected online to a Finnigan MAT 252 mass spectrometer. Isotope ratios were calibrated using NBS18 ($\delta^{13}C = -5.00‰$, $\delta^{18}O = -22.96‰$, relative to VPDB) and NBS19 ($\delta^{13}C = 1.95‰$, $\delta^{18}O = -2.20‰$, relative to VPDB). External reproducibility is better than ± 0.1‰ for $\delta^{13}C$ and ± 0.1‰ for $\delta^{18}O$ measurements. External reproducibility for carbonate concentration is better than ± 10%.

Density Separation

This method exploits the specific gravity of minerals. It is known that minerals with different specific gravity can be separated with a centrifuge by using a heavy liquid with a density in between the specific gravity of the selected minerals. In our case, aragonite is heavier (2.93 g/mL) than most minerals found in ash, and especially calcite (2.71 g/mL), and therefore it can be separated by density. We developed a tailored procedure based on a method for shell carbonates (Douka et al. 2010). We used sodium polytungstate (SPT) – $Na_6(H_2W_{12}O_{40})$ – as heavy liquid, which was purchased from TC-Tungsten Compounds GmbH (Germany) in a purified form poor in C and N isotopes (less than 100 ppm of carbon). High-density SPT has pH 3, which favors the dissolution of carbonates. Therefore, SPT was buffered with an aqueous solution at pH 8, obtained by mixing 93.2% of 1 M Na_2HPO_4 with 6.8% of 1 M NaH_2PO_4. The resulting solution has pH 7. Given the large variability in specific gravity of pyrogenic aragonite crystals (2.40–2.93 g/mL), we empirically established that 2.75 g/mL is the best density to reach highest efficiency in separating aragonite from lighter components. The bulk aragonite-rich sediment was dry sieved and 100 mg of the fraction smaller than 50 µm were placed in a 15-mL plastic tube. This powder was mixed with 300 µL of buffer solution and vortexed for a few seconds. After, 4 mL of SPT ($\rho = 2.86$ g/mL) were added and the solution was vortexed for a few seconds, resulting in a density $\rho = 2.75$ g/mL due to mixing of SPT with the buffer. The solution was placed in an ultrasonic bath for 10 min, vortexed for a few seconds, and then centrifuged for 20 min at 4000 rpm. The light fraction floating on SPT, which includes light minerals and organic components, was removed with a pipette. However, due to the high viscosity of SPT, it was not possible to remove completely the supernatant. Therefore, in order to preserve intact the heavy fraction, the tube was frozen with liquid N_2, and the tip trimmed using a hose cutter. After melting at ambient conditions, the solution was transferred to a 2 mL centrifuge tube and rinsed 3 times in deionized water using a centrifuge for 3 min at 5000 rpm. The efficiency of the procedure for this particular sample is ca. 30%. Finally, 1 mL of 0.1 M NaOH were added for 5 min to remove humic acids. The solution was clear, and therefore the sample was rinsed 3 times in deionized water using a centrifuge for 3 min at 5000 rpm, and air dried. Light and heavy fractions were analyzed with FTIR and XRD to check their mineralogy. The same procedure was used with the experimental aragonite-rich ash and geogenic aragonite.

https://doi.org/10.1017/RDC.2017.7 Published online by Cambridge University Press

SPT at higher density ($\rho = 2.90$ g/mL) was used on the heavy fraction obtained from the first round of separation to extract hydroxylapatite, which is heavier than aragonite (3.10 g/mL).

Thermogravimetric Analysis (TGA)

Samples were placed in an alumina crucible and combusted in air atmosphere from room temperature to 1000°C, at a heating rate of 20°C per min, using a SDT Q600 V8.3 Build 101 thermal analyzer.

^{14}C Dating

For the conventional carbonate dissolution method, 200 mg of the purified fraction were dissolved in phosphoric acid for 16 hr to evolve CO_2. For the step combustion dissolution, 200 mg of the purified fraction were placed in a quartz ampule under vacuum, and combusted using an electric oven to 550, 600, 700, and 800°C to evolve CO_2. Combustion steps lasted 1 hr, and for each step the evolved CO_2 was collected as a separate sample. The CO_2 released during heating up to 500°C was discarded to avoid possible contribution from residual organics. The different CO_2 fractions from acid dissolution and step combustion were converted into graphite for accelerator mass spectrometry (AMS) following Yizhaq et al. (2005). Two charred olive pits recovered from the black layer were treated with a general ABA procedure and the resulting product was combusted to evolve CO_2, which was converted to graphite for AMS using the same method (Yizhaq et al. 2005). AMS measurements were performed at the D-REAMS laboratory, Weizmann Institute of Science. A marble sample from Ness Ziona (Israel) was used as background. As no CO_2 was emitted at 550 and 600°C, the CO_2 collected at 700°C was used as background for the 550, 600, and 700°C ash samples. The 800°C fraction was used for the corresponding 800°C samples. Marble dissolved in phosphoric acid was used as background for the non-combusted ash samples. In case of small sample size (below 0.5 mg), oxalic acid II samples of similar size were used for normalization. Small and large background samples were measured, and linear extrapolation was used in order to estimate the best background for each sample size.

RESULTS

Formation Processes of the Destruction Horizon

FTIR analysis of the white ashy sediment revealed the dominant presence of aragonite, calcite, and quartz (SiO_2), together with minor amounts of hydroxylapatite [$Ca_5(PO_4)_3(OH)$], presumably from bone, and burnt clay minerals (Figure 2). The occurrence of the latter suggests that the sediment was exposed to temperatures above 600°C (Forget et al. 2015). This is in agreement with the phytolith assemblage of this layer, characterized by cereal inflorescence and leaf/stem morphotypes, many of which are melted due to heating at high temperature (Figure 3). The crystalline phases were analyzed using XRD, which confirmed that most of the bulk sediment is composed of aragonite and calcite, whereas quartz and hydroxylapatite occur in minor amounts. The fraction smaller than 50 μm contains mostly aragonite and a lesser amount of calcite compared to the bulk sediment (Figure 2 and Table 1).

Mineral and organic components were observed within their original depositional context using micromorphology (Figure 4A). Thin sections showed a diffuse boundary between the white aragonite-rich layer and the black layer, and similar microstructure, indicating that they could be two portions of the same depositional unit (Figure 4B). The only major difference is color, which is black in the lower part due to the presence of charred components from incomplete combustion of plant material, and white in the upper part as a result of near-surface, oxidizing

https://doi.org/10.1017/RDC.2017.7 Published online by Cambridge University Press

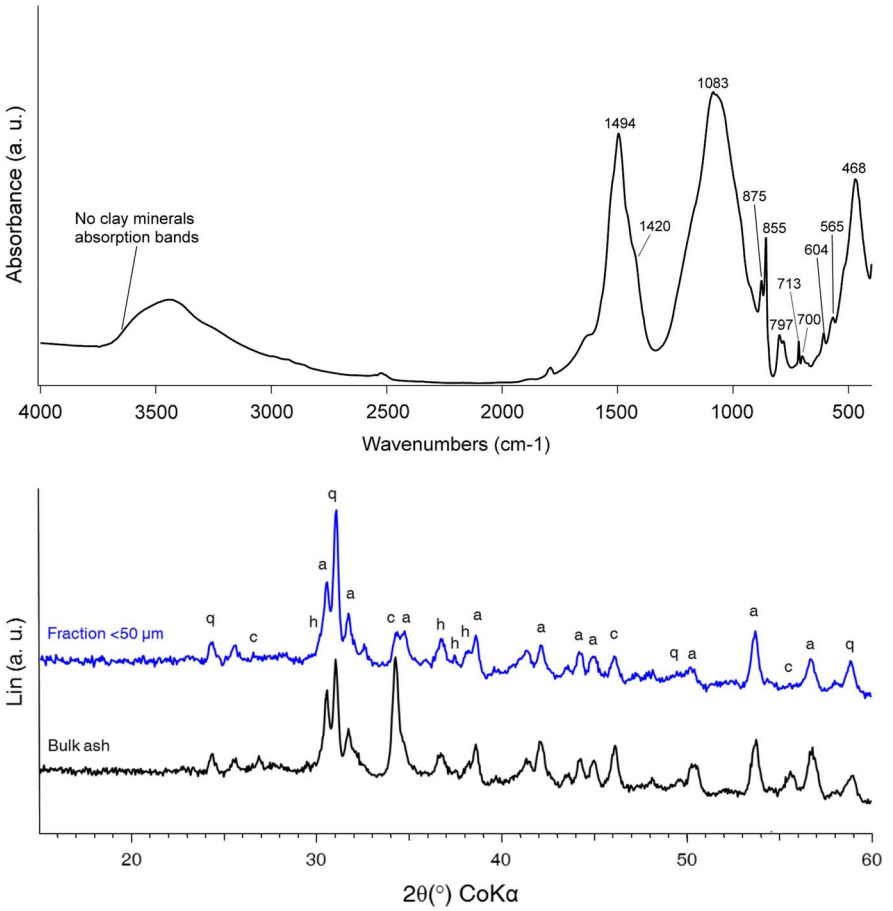

Figure 2 Mineralogical analyses. Top: FTIR spectrum of the white ashy layer (a. u.: arbitrary units). The absorption bands at 1494, 1083, 855, 713, and 700 cm^{-1} belong to aragonite. Calcite is represented by the absorption bands at 1420 (shoulder), 875 and 713 cm^{-1}. The latter indicates that calcite is enriched in magnesium. Other major components are quartz (1083 shared with aragonite, 797 and 468 cm^{-1}) and hydroxylapatite (604 and 565 cm^{-1}). Note the absence of absorption bands of clay minerals in the 3700–3600 cm^{-1} region, which is caused by exposure to high temperature. Bottom: diffractograms of the bulk aragonite-rich sediment and the fraction smaller than 50 µm (a. u.: arbitrary units). The main components are quartz (q), aragonite (a), calcite (c), and hydroxylapatite (h). Note that the amount of calcite decreases in the smaller fraction.

conditions that led to high-temperature burning. In the aragonite-rich portion (white layer), the mineral components are organized in intact, horizontally layered stringers of $CaCO_3$ aggregates showing the characteristic texture of high-temperature ash and lime plaster (Figure 4C). These ash aggregates also exhibit the structure of plant tissues, which is represented by phytoliths. Such degree of preservation points to absence of trampling and quick burial. Ash aggregates are surrounded by a large number of needle-shaped $CaCO_3$ crystals smaller than 50 µm (Figure 4D). These crystals were analyzed with µ-Raman spectrometry, confirming their identification as pure aragonite (Figure 5). Scanning electron microscope (SEM) images of the aragonite needles revealed that most of the crystals range between 1 and 10 µm in length and show intact facets, indicating good overall preservation (Figure 6A). Similar aragonite needles

https://doi.org/10.1017/RDC.2017.7 Published online by Cambridge University Press

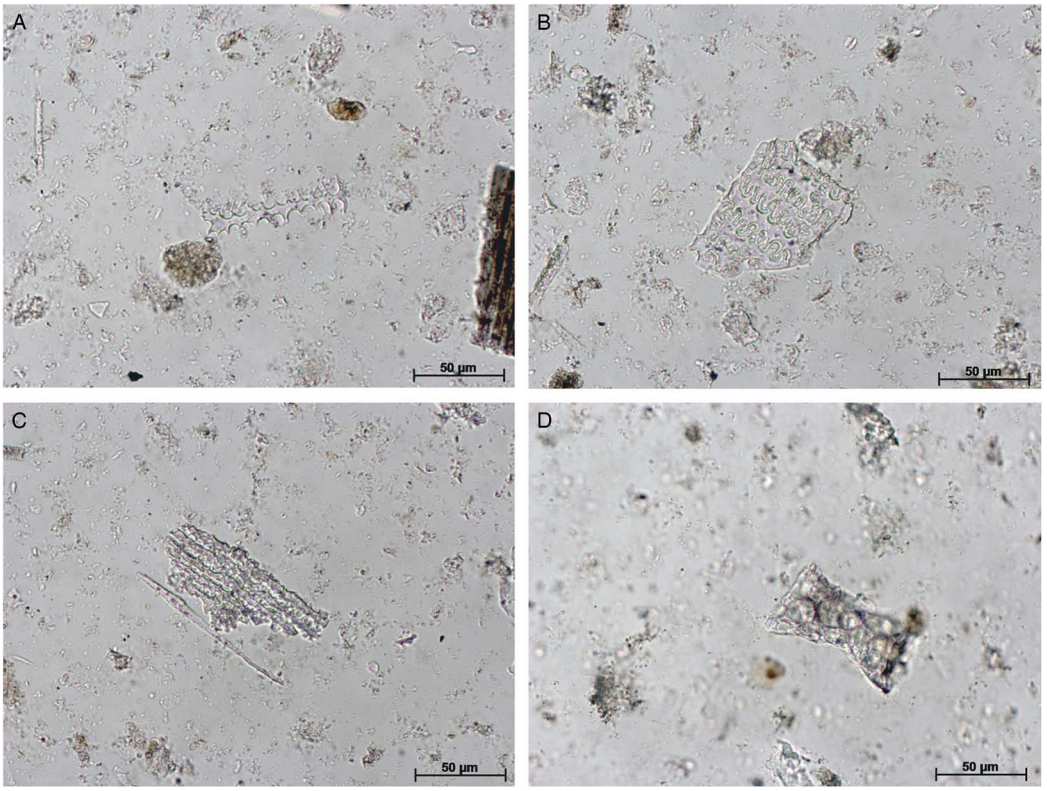

Figure 3 Photomicrographs in plane polarized light of opaline phytoliths extracted from the white (aragonite-rich) layer. A: dendritic phytolith from the inflorescence of cereals. B: multicell composed of dendritic phytoliths, from the inflorescence of cereals. C: multicell composed of echinate long cell phytoliths from the inflorescence of cereals (note the irregular appearance caused by partial melting at high temperature). D: melted phytolith characterized by irregular shape and bubbles produced by the escape of water during exposure to high temperature.

Table 1 Quantitative XRD analysis of the white layer rich in aragonite (in wt% of the crystalline phases). Note that these results do not include disordered phases such as burnt clay minerals, opal from phytoliths and highly irregular hydroxylapatite crystals.

Mineral phase	Bulk	Fraction <50 µm
Aragonite	37	47
Calcite	36	16
Quartz	15	20
Hydroxylapatite	12	17

were observed in experimental ash and therefore we conclude that the aragonite phase in the white layer is pyrogenic (Figure 6B). All of these lines of evidence suggest that plant material, a mixture of chaff and straw, was laid on the surface of an open area—a practice observed elsewhere at the site (Regev et al. 2015). This vegetal cover was burnt to high temperature during the destruction event. Plant calcium oxalate and geogenic calcite from local sediments transformed into CaO, which turned into aragonite upon carbonation as soon as the

https://doi.org/10.1017/RDC.2017.7 Published online by Cambridge University Press

Figure 4 Micromorphology of sediments. A: photo of the micromorphology block before removal. A thin section was obtained from the area highlighted by the dashed rectangle (scale bar: 5 cm). B: scan of the thin section prepared from the portion of the block highlighted in (A), showing the microstratigraphy of the sample (scale bar: 1 cm). 1: burnt mudbrick collapse; 2: white (aragonite-rich) layer; 3: black layer. Note the diffuse boundary between the white and black layers. C: photomicrograph of the white layer showing the horizontal stringers of ash (PPL; scale bar: 1 mm). Note the presence of a large fragment of chalk in between stringers. D: photomicrograph of the white layer showing needle-shaped crystals of $CaCO_3$ (XPL; scale bar: 100 μm).

https://doi.org/10.1017/RDC.2017.7 Published online by Cambridge University Press

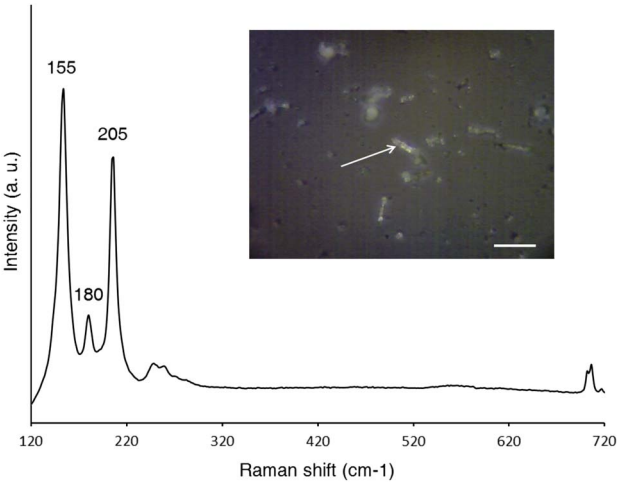

Figure 5 Raman spectrum of a representative needle-shaped crystal from the white (aragonite-rich) layer (indicated by an arrow in the inset), showing Raman bands of aragonite at 155, 180, and 205 cm^{-1} (scale bar: 20 μm; a. u.: arbitrary units).

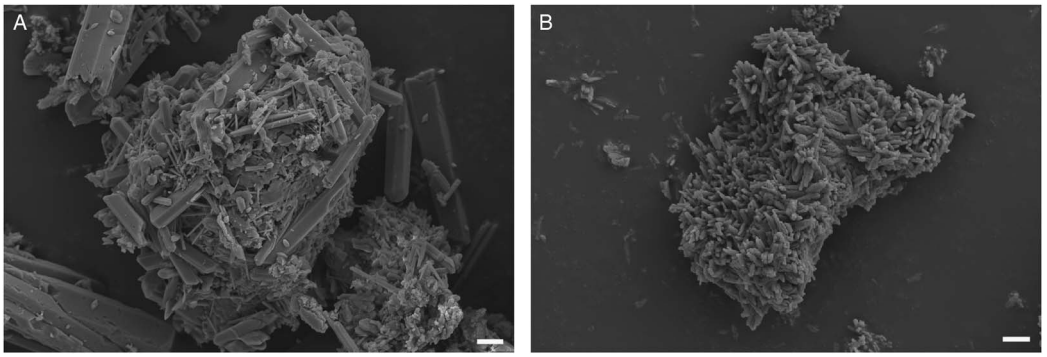

Figure 6 SEM images of archaeological and experimental samples. A: cluster of needle-shaped aragonite crystals from the white (aragonite-rich) layer (scale bar: 1 μm). Note that small, thin crystals are surrounded by larger ones with well-developed facets. B: experimental ash rich in clusters of needle-shaped crystals of pyrogenic aragonite (scale bar: 1 μm).

combustion temperature dropped below 100°C, towards the end of the conflagration. The ash layer was then buried by mudbrick debris, which favored the preservation of aragonite crystals. This finds support in the absence of sparitic $CaCO_3$ crystals in thin section, suggesting that ash was not affected by dissolution and reprecipitation processes, and thus it is well preserved. This observation is in disagreement with the $\delta^{13}C$ and $\delta^{18}O$ values of the carbonate fraction, which fall outside the range of high-temperature ash as shown in Table 2 (Shahack-Gross and Ayalon 2013 and references therein). Considering that the site is located on top of a chalk hill, we conclude that the stable isotopes results are affected by the presence of geogenic calcite. This phase is devoid of ^{14}C and therefore it is a contaminant for ^{14}C dating (Figure 4C). Similarly, hydroxylapatite from bone mineral might be rich in geogenic carbonate groups due to diagenetic processes. Thus, aragonite must be separated from these phases in order to obtain accurate age determinations.

https://doi.org/10.1017/RDC.2017.7 Published online by Cambridge University Press

Table 2 Carbon and oxygen stable isotopes values of archaeological and control samples. Values for high-temperature carbonates are based on published data (Shahack-Gross and Ayalon 2013 and references therein).

Sample ID	$\delta^{13}C$ (‰ VPDB)	$\delta^{18}O$ (‰ VPDB)
Tel Megiddo chalk	0.01	–2.23
White layer (aragonite-rich)	–13.60	–5.40
High-temperature carbonates	–20.00/–13.00	–21.00/–14.00

Density Separation and ^{14}C Dating

Aragonite needles were extracted from the ash fraction smaller than 50 μm through density separation of minerals with different specific gravity, using sodium polytungstate (SPT) as heavy liquid. By centrifuging the sample in buffered SPT at density $\rho = 2.75$ g/mL and pH 7, most of the aragonite is concentrated in the heavy fraction, together with heavy minerals and heat-altered hydroxylapatite. FTIR and XRD show also the possible presence of a small amount of calcite, although the relative infrared absorptions and X-ray reflections are weak (Figure 7). After further separating hydroxylapatite from aragonite at 2.90 g/mL density, we ascertained with FTIR that the former is not carbonated due to exposure to fire, and therefore it cannot be a contaminant (Figure 8). We then proceeded to dissolution of the purified samples in phosphoric acid and graphitization of CO_2 following Yizhaq et al. (2005). The ^{14}C content of fractions with different specific gravity was measured by AMS. In addition, we measured two charred olive pits found together within the black layer. Measurements were evaluated against a published reference dataset of age determinations based on clusters of charred olive pits (Toffolo et al. 2014). Results are presented in Table 3.

The robustness of the density separation method is supported by the measurement on experimental ash, which excludes contribution of dead carbon from SPT, and the measurement on ^{14}C-dead geogenic aragonite, which shows no contamination from modern carbon due to sample preparation and the NaOH step. The bulk ash appears to be much older than the fraction smaller than 50 μm, likely because of the presence of coarse-grained calcite from weathered chalk. Both samples do not match the age of olive pits. The fraction lighter than 2.65 g/mL is largely outside the expected pMC range, as a result of the occurrence of geogenic calcite from local sediments. A similar situation characterizes the fraction lighter than 2.75 g/mL, although the presence of a larger amount of aragonite accounts for the higher pMC. The fractions heavier than 2.75 g/mL, where most of the aragonite is located, exhibit the closest pMC values compared to the reference samples, thus establishing a direct correlation between specific gravity and ^{14}C age. These values are ca. 100 yr BP older than expected. This discrepancy might be caused by incomplete removal of calcite during SPT treatment, as hinted by FTIR and XRD. In fact, a contamination value as low as 1% could account for the observed age shift (Bowman 1990). Therefore, instead of dissolving the purified fraction in phosphoric acid, the sample was combusted under vacuum. It is known that the decomposition temperature of $CaCO_3$ is related to the degree of atomic order of the crystal, with well-ordered crystals decomposing at higher temperature (Cuif et al. 2004; Stalport et al. 2007; Lindroos et al. 2012). This implies that pyrogenic aragonite, a disordered type of $CaCO_3$, releases CO_2 at lower temperature compared to geogenic calcite. This property was observed in the sample under study using TGA, which showed that the Tel Megiddo ash starts decomposing at 500°C, whereas local chalk releases CO_2 only above 600°C (Figure 9). By heating the sample at different temperatures, a clear trend emerges from the pMC values (Figure 10). The CO_2

https://doi.org/10.1017/RDC.2017.7 Published online by Cambridge University Press

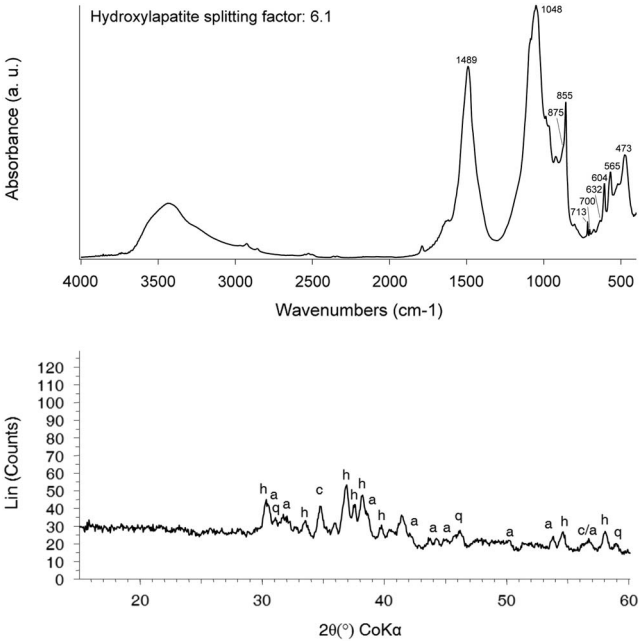

Figure 7 Mineralogical analyses on purified fractions. Top: FTIR spectrum of the heavy fraction separated using SPT at 2.75 g/mL density (a. u.: arbitrary units). Dominant phases are pyrogenic aragonite (absorption bands at 1489, 855, 713, and 700 cm^{-1}) and hydroxylapatite (1048, 632, 604, and 565 cm^{-1}). The high splitting factor (6.1) and the presence of the 632 cm^{-1} absorption band indicate that hydroxylapatite was exposed to high temperature. Minor phases are quartz (473 cm^{-1}) and possibly calcite (shoulder at 875 cm^{-1}). Bottom: diffractogram of the heavy fraction separated using SPT at 2.75 g/mL density. Note the presence of aragonite (a), hydroxylapatite (h), quartz (q), and possibly calcite (c).

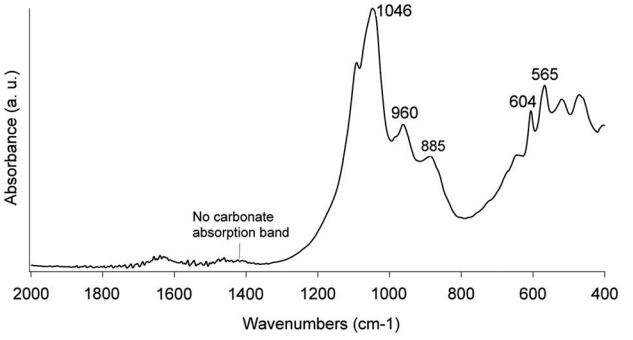

Figure 8 FTIR spectrum of the heavy fraction separated using SPT at 2.90 g/mL density (a. u.: arbitrary units). The dominant phase is hydroxylapatite. Note the absence of the carbonate $\nu 3$ absorption band in the 1490–1420 cm^{-1} region, indicating exposure to high temperature.

evolved at 550°C, which belongs to the aragonite phase, matches the pMC values of charred olive pits and thus falls within the expected range of the destruction horizon, whereas the CO_2 evolved at higher temperature shows progressively lower pMC values, due to the contribution

https://doi.org/10.1017/RDC.2017.7 Published online by Cambridge University Press

Table 3 ^{14}C dating results, showing laboratory number, preparation method, material, size, pMC, and ^{14}C age. The last row lists published samples used as reference (Toffolo et al. 2014).

Lab nr	Sample nr in Figure 10	Preparation method	Material	Size (mg C)	pMC	^{14}C age ± 1σ BP
RTD-8141	—	SPT + NaOH + phosphoric acid	Experimental ash	1.29	101.82 ± 0.27	—
RTD-8808	—	SPT + NaOH + phosphoric acid	Aragonite spar	1.00	0.253 ± 0.03	48040 ± 900
RTD-8580	1	SPT + NaOH + phosphoric acid	Bulk ash	1.00	57.01 ± 0.21	4510 ± 30
RTD-8581	2	SPT + NaOH + phosphoric acid	Ash <50 µm	1.02	64.36 ± 0.29	3540 ± 35
RTD-8514	3	SPT + NaOH + phosphoric acid	Ash <2.65 g/mL	1.00	63.48 ± 0.20	3650 ± 25
RTD-8582	4	SPT + NaOH + phosphoric acid	Ash <2.75 g/mL	1.00	64.71 ± 0.22	3495 ± 25
RTD-8583	5	SPT + NaOH + phosphoric acid	Ash >2.75 g/mL, <2.90 g/mL	0.98	68.17 ± 0.21	3075 ± 25
RTD-8584	6	SPT + NaOH + phosphoric acid	Ash >2.90 g/mL	0.17	68.56 ± 0.32	3030 ± 35
RTD-8633.1	7	SPT + NaOH + step combustion	Ash >2.75 g/mL, 550°C	0.32	70.67 ± 0.23	2790 ± 25
RTD-8633.2	8	SPT + NaOH + step combustion	Ash >2.75 g/mL, 600°C	0.27	69.06 ± 0.27	2975 ± 30
RTD-8633.3	9	SPT + NaOH + step combustion	Ash >2.75 g/mL, 700°C	1.00	68.32 ± 0.28	3060 ± 35
RTD-8639.1	10	SPT + NaOH + step combustion	Ash <2.75 g/mL, 550°C	0.42	70.52 ± 0.22	2805 ± 25
RTD-8639.2	11	SPT + NaOH + step combustion	Ash <2.75 g/mL, 600°C	0.58	67.12 ± 0.20	3200 ± 25
RTD-8639.3	12	SPT + NaOH + step combustion	Ash <2.75 g/mL, 700°C	1.00	63.68 ± 0.21	3625 ± 25
RTD-8639.4	13	SPT + NaOH + step combustion	Ash <2.75 g/mL, 800°C	0.10	52.83 ± 0.25	5125 ± 35
RTD-8603 and RTD-8604	—	Acid-base-acid	Charred olive pits from black layer	N/A	69.39–70.33	2935–2825
RTT-3939, 3940, 3942, 3943, 3944, 3945, 3946, 5089, 5496, 5497; RTK-6273, 6274	—	Acid-base-acid	Charred olive pits from Iron Age I destruction horizon (Area K, M, H)	N/A	69.59–70.93	2920–2760

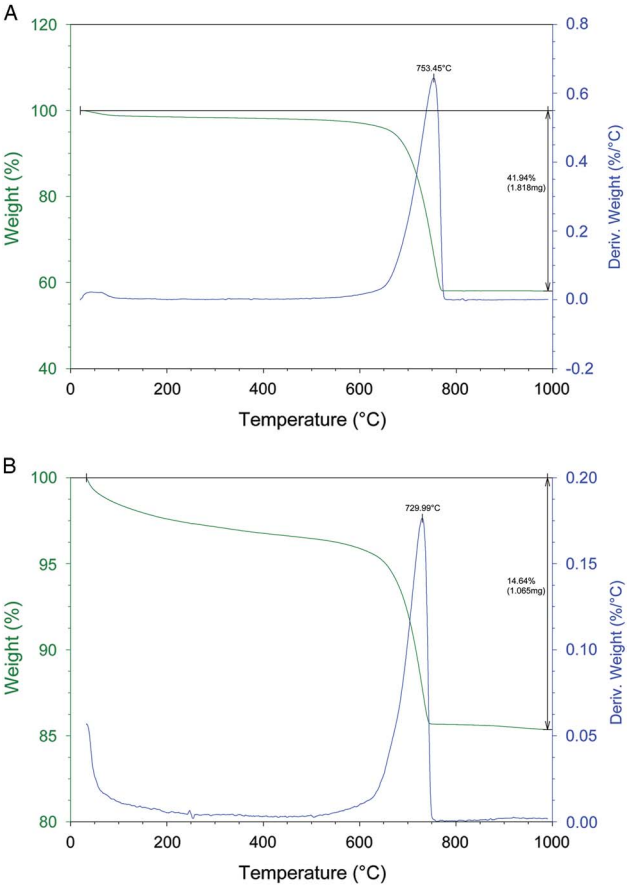

Figure 9 TGA plots of bedrock chalk from Tel Megiddo (A) and the aragonite-rich layer (B). Note that the latter starts decomposing at lower temperature compared to chalk.

of geogenic calcite. A similar pattern was observed for the fraction lighter than 2.75 g/mL, which contains a small, yet significant amount of aragonite.

DISCUSSION

The ^{14}C dating results demonstrate that pyrogenic aragonite is a closed carbon system that records the ^{14}C signature of the atmosphere in the moment it nucleates, shortly after a firing event. Even though aragonite is thermodynamically unstable at ambient temperatures and pressures, meaning that it will eventually recrystallize into calcite with possible isotopic exchange (Lippmann 1973), this condition largely depends on environmental factors such as presence of water and low pH. In fact, aragonite can survive intact for a long time, as in the case of the nautiloid shells from the Buckhorn asphalt quarry, dated to ca. 300 million yr ago (Seuss et al. 2012), and the crystals embedded in chondrite meteorites from 4.6 billion yr ago (Lee and Lindgren 2015). In both instances, the absence of water left aragonite essentially pristine.

Similar settings must have determined the preservation of aragonite at Tel Megiddo, where it provided accurate age determinations as seen from pMC values. Tel Megiddo is located within

https://doi.org/10.1017/RDC.2017.7 Published online by Cambridge University Press

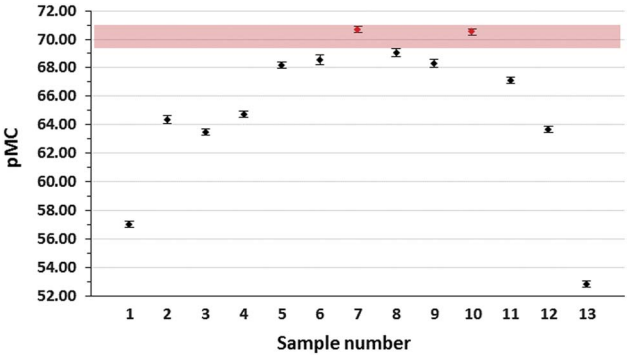

Figure 10 pMC values for the archaeological samples treated with acid dissolution and step combustion (sample numbers are listed in Table 3). The shaded bar indicates the expected pMC range of the destruction horizon based on measurements carried out on charred seeds from the black layer and from other locations at Tel Megiddo (Toffolo et al. 2014). Note that the only samples that fall within this range are those produced by combusting purified aragonite-rich ash at 550°C.

the Mediterranean climate zone and receives an amount of precipitations comparable to southern and western Europe (e.g. Mehta and Yang 2008). Considering that the aragonite layer is located about two meters below the topsoil (Figure 1B), we infer that the thick mudbrick collapse has favored the preservation of aragonite from rainwater seeping through the section. The large amount of clay in this layer is especially important, as more porous sandy sediments might lead to in-depth penetration of rainwater and movement of groundwater. Therefore, we conclude that aragonite could occur also in temperate zones elsewhere around the world, provided that it is not close to the topsoil and embedded in sandy sediments at open-air sites.

Accurate ^{14}C dating of pyrogenic aragonite was accomplished through a careful characterization of the depositional context, including bulk analyses (FTIR, XRD, phytoliths) and descriptions of intact portions of sediment (micromorphology) to reconstruct the formation processes of the destruction horizon, understand the preservation status of sediments, and verify the occurrence of contaminants. In addition, μ-Raman provided the first spectroscopic characterization of single pyrogenic aragonite needles in archaeological sediments. Thus, the link between experimental and archaeological samples suggested in a previous study is now confirmed (Toffolo and Boaretto 2014). With this approach, we were able to locate and target one specific carbonate compound for ^{14}C dating. Currently, this is not the rule in ^{14}C dating of anthropogenic carbonates such as lime plasters and mortars, as usually a mixture of different carbonate phases provides the CO_2 for AMS measurements, thus leading to contradicting results in several cases (Lindroos et al. 2007; Boaretto and Poduska 2013; Ringbom et al. 2014). The target compound was extracted from the bulk sediment using density separation in a heavy liquid, an established method in geochemistry and ^{14}C dating of shell carbonates (Douka et al. 2010). We do note, however, that in the case of pyrogenic aragonite the needles are characterized by a high ratio of surface area to volume, and therefore dissolve almost immediately in high-density SPT, which is at pH 3. This would be negligible if the sample was 100% $CaCO_3$ as in shells, but it is a major shortcoming in the case of heterogeneous sediments such as ash. This problem was overcome by adding a buffer based on a mixture of different sodium phosphates that shifts the pH of SPT to 7. AMS measurements on fractions with different densities clearly showed that calcite is a major source of contamination due to its geologic origin

https://doi.org/10.1017/RDC.2017.7 Published online by Cambridge University Press

as a weathering product of chalk, whereas aragonite-rich fractions exhibit younger ^{14}C ages. The fact that the latter are 100 yr BP off compared to the expected age of the destruction horizon points to incomplete removal of calcite. This calcite phase is presumably attached to heavier aragonite crystals, thus resulting in a "composite" specific gravity that falls within the range of aragonite. For this reason, dissolution in phosphoric acid was replaced with step combustion under vacuum, which should also overcome the contribution of carbonate hydroxylapatite from bones (Stiner et al. 1995). A direct correlation between temperature and ^{14}C age emerges from AMS measurements, in both the heavy and light fractions of the ash. This is the result of decomposition of aragonite at 550°C, followed by the decomposition of a progressively larger amount of geogenic calcite at higher temperatures, which "dilutes" the ^{14}C content of aragonite. Considering that most of the carbonates in the purified fraction are aragonite crystals, it seems that part of such crystals decompose above 550°C together with calcite. This might be due to a higher degree of atomic order within the crystal lattice, as in the case of needles larger than 20 μm observed with SEM, which presumably reached their size through a relatively slow and steady growth process.

Our results show that pyrogenic aragonite is a new short-lived material suitable for ^{14}C dating. The occurrence of pyrogenic aragonite has been recently documented in several combustion features and lime plasters found at archaeological sites of different age located in Israel (Toffolo and Boaretto 2014: Table 1). This limited geographic distribution is due to the fact that pyrogenic aragonite is best identified using FTIR, but this method has been used sparingly in other parts of the world (Weiner 2010). Given the presence of archaeological pyrogenic aragonite in different sedimentary contexts and chronological periods spanning the last 30,000 yr, we believe that its occurrence could be much more widespread than thought. For this reason, the dating method presented here could find extensive applications, regardless of geographic location and chronological period, up to the limit of ^{14}C. Once aragonite has been identified, it is necessary to exclude possible sources of contamination. The main ones are geogenic calcite and diagenetic carbonates, such as carbonate hydroxylapatite and reprecipitated calcite. The possible presence of secondary calcite does not exclude the presence of aragonite. This is because diagenesis does not affect sediments homogeneously, and pockets of pristine aragonite may survive next to areas rich in secondary calcite within the same layer of sediment. This is a common situation in caves (e.g. Karkanas et al. 2000; Weiner et al. 2002). As a general rule of thumb, one should keep in mind that each ash deposit is characterized by a unique mineral assemblage, and therefore SPT density should be adjusted case by case to identify the fraction most suitable for step combustion. This in turn requires a thorough understanding of formation processes. Using this approach, a number of common archaeological features and materials involving the use of fire could be accurately dated, provided that aragonite is preserved: destruction horizons, hearths, cooking installations, lime kilns, furnaces, metal workshops, limestone-tempered pottery, lime plasters, and mortars. These features and artifacts are directly related to short-lived human activities, and thus could significantly contribute to the establishment of accurate ^{14}C chronologies together with organic materials, or in their absence. Furthermore, pyrogenic aragonite could be a viable alternative to the current ^{14}C dating method applied to lime mortars, which showed its limits due to the often altered isotopic composition of calcite and the inability to target one specific carbonate compound (Boaretto and Poduska 2013).

Finally, we wish to note that also high-temperature calcite might preserve the original ^{14}C signature of the atmosphere, similar to pyrogenic aragonite. In the cases where pyrogenic aragonite does not nucleate after fire due to adverse environmental conditions, high-temperature calcite could be used for ^{14}C dating. This calcite fraction is extremely disordered

at the atomic level and thus it is lighter than diagenetic or geogenic calcite, which might occur within the same layer of sediment. Therefore, it can be extracted by density separation using the same procedure developed for aragonite. This would extend the application of the method presented herein to several other anthropogenic carbonate materials in which aragonite is not present.

ACKNOWLEDGMENTS

This research was funded by the Alexander von Humboldt Foundation through postdoctoral fellowship to Michael Toffolo, which included a Europe Research Stay at the Weizmann Institute of Science. Part of the FTIR measurements were performed on instrumentation funded by a grant from the Deutsche Forschungsgemeinschaft (MI 1748/1-1). Sample preparation for ^{14}C dating was funded by the Exilarch's Foundation for the Dangoor Research Accelerator Mass Spectrometer and by the Max Planck-Weizmann Center for Integrative Archaeology and Anthropology. Micromorphological analysis was conducted by RSG at the Kimmel Center for Archaeological Science, Weizmann Institute of Science. The authors are grateful to Israel Finkelstein and Mario Martin, co-directors of the Megiddo Expedition, for granting access to the site, and to Heinrich Taubald for performing stable isotopes analysis. CB wishes to thank Frieder Lauxmann for performing μ-Raman measurements. MBT wishes to thank Francesca Strappini for her continued support during laboratory analyses and writing, Steve Weiner and Yotam Asscher for useful discussions, and Ilit Cohen-Ofri for assistance during TGA analysis.

REFERENCES

Adler DS, Bar-Yosef O, Belfer-Cohen A, Tushabramishvili N, Boaretto E, Mercier N, Valladas H, Rink WJ. 2008. Dating the demise: Neandertal extinction and the establishment of modern humans in the southern Caucasus. *Journal of Human Evolution* 55:817–33.

Albert RM, Ruíz JA, Sans A. 2016. PhytCore ODB: a new tool to improve efficiency in the management and exchange of information on phytoliths. *Journal of Archaeological Science* 68:98–105.

Asscher Y, Lehmann G, Rosen SA, Weiner S, Boaretto E. 2015a. Absolute dating of the Late Bronze to Iron Age transition and the appearance of Philistine culture in Qubur el-Walaydah, southern Levant. *Radiocarbon* 57(1):77–97.

Asscher Y, Cabanes D, Hitchcock LA, Maeir AM, Weiner S, Boaretto E. 2015b. Radiocarbon dating shows an early appearance of Philistine material culture in Tell es-Safi/Gath, Philistia. *Radiocarbon* 57:825–50.

Berna F, Goldberg P, Kolska Horwitz L, Brink J, Holt S, Bamford M, Chazan M. 2012. Microstratigraphic evidence of in situ fire in the Acheulean strata of Wonderwerk Cave, Northern Cape province, South Africa. *PNAS* 109:E1215–E20.

Boaretto E, Poduska KM. 2013. Materials science challenges in radiocarbon dating: the case of archaeological plasters. *Journal of the Minerals, Metals & Materials Society* (TMS) 65:481–8.

Bowman S. 1990. *Radiocarbon Dating*. London: British Museum Press.

Boynton RS. 1980. *Chemistry and Technology of Lime and Limestone*. New York: John Wiley & Sons, Inc.

Cohen-Ofri I, Weiner L, Boaretto E, Mintz G, Weiner S. 2006. Modern and fossil charcoal: aspects of structure and diagenesis. *Journal of Archaeological Science* 33(3):428–39.

Courty MA, Goldberg P, Macphail RI. 1989. *Soils and Micromorphology in Archaeology*. Cambridge: Cambridge University Press.

Cuif J-P, Dauphin Y, Berthet P, Jegoudez J. 2004. Associated water and organic compounds in coral skeletons: quantitative thermogravimetry coupled to infrared absorption spectrometry. *Geochemistry, Geophysics, Geosystems* 5:Q11011.

Douka K, Hedges REM, Higham TFG. 2010. Improved AMS ^{14}C dating of shell carbonates using high-precision X-ray diffraction and a novel density separation protocol (CarDS). *Radiocarbon* 52:735–51.

Farmer VC, editor. 1974. *The Infrared Spectra of Minerals*. London: Mineralogical Society.

Finkelstein I, Ussishkin D, Halpern B, editors. 2000. *Megiddo III. The 1992–1996 Seasons*. Tel Aviv: Emery and Claire Yass Publications in Archaeology.

Finkelstein I, Ussishkin D, Halpern B, editors. 2006. *Megiddo IV. The 1998–2002 Seasons*. Tel Aviv: Emery and Claire Yass Publications in Archaeology.

Finkelstein I, Ussishkin D, Cline EH, editors. 2013. *Megiddo V. The 2004–2008 Seasons*. Tel Aviv: Emery and Claire Yass Publications in Archaeology.

Forget MCL, Regev L, Friesem DE, Shahack-Gross R. 2015. Physical and mineralogical properties of experimentally heated chaff-tempered mud bricks: implications for reconstruction of environmental

factors influencing the appearance of mud bricks in archaeological conflagration events. *Journal of Archaeological Science: Reports* 2:80–93.

Franceschi VR, Nakata PA. 2005. Calcium oxalate in plants: formation and function. *Annual Review of Plant Biology* 56:41–71.

Frost RL, Weier ML. 2004. Thermal treatment of whewellite – a thermal analysis and Raman spectroscopic study. *Thermochimica Acta* 409: 79–85.

Gowlett JAJ, Wrangham RW. 2013. Earliest fire in Africa: towards the convergence of archaeological evidence and the cooking hypothesis. *Azania: Archaeological Research in Africa* 48:5–30.

Karkanas P, Bar-Yosef O, Goldberg P, Weiner S. 2000. Diagenesis in prehistoric caves: the use of minerals that form in situ to assess the completeness of the archaeological record. *Journal of Archaeological Science* 27(10):915–29.

Katz O, Cabanes D, Weiner S, Maeir AM, Boaretto E, Shahack-Gross R. 2010. Rapid phytolith extraction for analysis of phytolith concentrations and assemblages during an excavation: an application at Tell es-Safi/Gath, Israel. *Journal of Archaeological Science* 37(7):1557–63.

Koumouzelis M, Ginter B, Kozlowski JK, Pawlikowski M, Bar-Yosef O, Albert RM, Litynska-Zajac M, Stworzewicz E, Wojtal P, Lipecki G, Tomek T, Bochenski ZM, Pazdur A. 2001. The early Upper Palaeolithic in Greece: the excavations in Klisoura Cave. *Journal of Archaeological Science* 28:515–39.

Kuhn SL, Stiner MC, Güleç E, Özer I, Yılmaz H, Baykara I, Açıkkol A, Goldberg P, Molina KM, Ünay E, Suata-Alpaslan F. 2009. The early Upper Paleolithic occupations at Üçağızlı Cave (Hatay, Turkey). *Journal of Human Evolution* 56(2): 87–113.

Lee MR, Lindgren P. 2015. 4.6-billion-year-old aragonite and its implications for understanding the geological record of Ca-carbonate. *Carbonates and Evaporites* 30:477–81.

Lindroos A, Heinemeier J, Ringbom Å, Braskén M, Sveinbjörndóttir Á. 2007. Mortar dating using AMS ^{14}C and sequential dissolution: examples from medieval, non-hydraulic lime mortars from the Åland Islands, SW Finland. *Radiocarbon* 49(1):47–67.

Lindroos A, Regev L, Oinonen M, Ringbom Å, Heinemeier J. 2012. ^{14}C dating of fire-damaged mortars from medieval Finland. *Radiocarbon* 54(3):915–32.

Lippmann F. 1973. *Sedimentary Carbonate Minerals*. Heidelberg: Springer.

Madella M, Alexandre A, Ball T. 2005. International Code for Phytolith Nomenclature 1.0. *Annals of Botany* 96:253–60.

Mehta AV, Yang S. 2008. Precipitation climatology over Mediterranean Basin from ten years of TRMM measurements. *Advances in Geosciences* 17:87–91.

Mulholland SC, Rapp GJ. 1992. Phytolith systematics: an introduction. In: Rapp JG, Mulholland SC, editors. *Phytolith Systematics: Emerging Issues*. New York: Plenum Press. p 1–13.

Price D, Dollimore D, Fatemi NS, Whitehead R. 1980. Mass spectrometric determination of kinetic parameters for solid state decomposition reactions. Part 1. Method; calcium oxalate decomposition. *Thermochimica Acta* 42:323–32.

Rebollo NR, Cohen-Ofri I, Popovitz-Biro R, Bar-Yosef O, Meignen L, Goldberg P, Weiner S, Boaretto E. 2008. Structural characterization of charcoal exposed to high and low pH: implications for ^{14}C sample preparation and charcoal preservation. *Radiocarbon* 50(2):289–307.

Rebollo NR, Weiner S, Brock F, Meignen L, Goldberg P, Belfer-Cohen A, Bar-Yosef O, Boaretto E. 2011. New radiocarbon dating of the transition from the Middle to the Upper Paleolithic in Kebara Cave, Israel. *Journal of Archaeological Science* 38:2424–33.

Regev J, Finkelstein I, Adams MJ, Boaretto E. 2014. Wiggle-matched ^{14}C chronology of Early Bronze Megiddo and the synchronization of Egyptian and Levantine chronologies. *Egypt and the Levant* 24:243–66.

Regev L, Eckmeier E, Mintz E, Weiner S, Boaretto E. 2011. Radiocarbon concentrations of wood ash calcite: potential for dating. *Radiocarbon* 53(1): 117–27.

Regev L, Cabanes D, Homsher R, Kleiman A, Weiner S, Finkelstein I, Shahack-Gross R. 2015. Geoarchaeological Investigation in a Domestic Iron Age Quarter, Tel Megiddo, Israel. *Bulletin of the American Schools of Oriental Research* 374: 135–57.

Ringbom Å, Lindroos A, Heinemeier J, Sonck-Koota P. 2014. 19 years of mortar dating: learning from experience. *Radiocarbon* 56(2):619–35.

Roebroeks W, Villa P. 2011. On the earliest evidence for habitual use of fire in Europe. *PNAS* 108: 5209–14.

Seuss B, Titshack J, Seifert S, Neubauer J, Nützel A. 2012. Oxygen and stable carbon isotopes from a nautiloid from the middle Pennsylvanian (Late Carboniferous) impregnation *Lagerstätte* "Buckhorn Asphalt Quarry" – Primary paleo-environmental signals versus diagenesis. *Palaeogeography, Palaeoclimatology, Palaeoecology* 319–320:1–15.

Shahack-Gross R, Ayalon A. 2013. Stable carbon and oxygen isotopic compositions of wood ash: an experimental study with archaeological implications. *Journal of Archaeological Science* 40:570–8.

Shahack-Gross R, Berna F, Karkanas P, Lemorini C, Gopher A, Barkai R. 2014. Evidence for the repeated use of a central hearth at Middle Pleistocene (300 ky ago) Qesem Cave, Israel. *Journal of Archaeological Science* 44:12–21.

Stalport F, Coll P, Szopa C, Person A, Navarro-Gonzalez R, Cabane M, Ausset P, Vaulay MJ. 2007. Search for past life on Mars: Physical and

https://doi.org/10.1017/RDC.2017.7 Published online by Cambridge University Press

chemical characterization of minerals of biotic and abiotic origin: 2. Aragonite. *Geophysical Research Letters* 34:L24102.

Stiner MC, Kuhn SL, Weiner S, Bar-Yosef O. 1995. Differential burning, recrystallization, and fragmentation of archaeological bone. *Journal of Archaeological Science* 22:223–37.

Stoops G, Marcelino V, Mees F, editors. 2010. *Interpretation of Micromorphological Features of Soils and Regoliths*. Amsterdam: Elsevier.

Taylor RE, Bar–Yosef O. 2014. *Radiocarbon Dating: An Archaeological Perspective*. Walnut Creek, CA: Left Coast Press.

Toffolo M, Maeir AM, Chadwick JR, Boaretto E. 2012. Characterization of contexts for radiocarbon dating: results from the early Iron Age at Tell es-Safi/Gath, Israel. *Radiocarbon* 54(3–4):371–90.

Toffolo MB, Arie E, Martin MAS, Boaretto E, Finkelstein I. 2014. Absolute chronology of Megiddo, Israel in the Late Bronze and Iron Ages: high-resolution radiocarbon dating. *Radiocarbon* 56(1):221–44.

Toffolo MB, Boaretto E. 2014. Nucleation of aragonite upon carbonation of calcium oxide and calcium hydroxide at ambient temperatures and pressures: a new indicator of fire-related human activities. *Journal of Archaeological Science* 49:237–48.

Twiss PC, Suess E, Smith RM. 1969. Morphological classification of grass phytoliths. *Soil Science Society of America* 33:109–15.

van der Marel HW, Beutelspacher H. 1976. *Atlas of Infrared Spectroscopy of Clay Minerals and Their Admixtures*. Amsterdam: Elsevier Scientific Publishing Company.

Wadley L, Sievers C, Bamford M, Goldberg P, Berna F, Miller CE. 2011. Middle Stone Age bedding construction and settlement patterns at Sibudu, South Africa. *Science* 334:1388–91.

Walker MJ, Anesin D, Angelucci DE, Avilés-Fernández A, Berna F, Buitrago-López AT, Fernández-Jalvo Y, Haber-Uriarte M, López-Jiménez A, López-Martínez M, Martín-Lerma I, Ortega-Rodrigáñez J, Polo-Camacho J-L, Rhodes SE, Richter D, Rodríguez-Estrella T, Schwenniger J-L, Skinner AR. 2016. Combustion at the late Early Pleistocene site of Cueva Negra del Estrecho del Río Quípar (Murcia, Spain). *Antiquity* 90:571–89.

Weiner S, Bar-Yosef O. 1990. States of Preservation of Bones from Prehistoric Sites in the Near East: a Survey. *Journal of Archaeological Science* 17: 187–96.

Weiner S, Goldberg P, Bar-Yosef O. 2002. Three-dimensional distribution of minerals in the sediments of Hayonim Cave, Israel: diagenetic processes and archaeological implications. *Journal of Archaeological Science* 29(11):1289–308.

Weiner S. 2010. *Microarchaeology. Beyond the Visible Archaeological Record*. New York: Cambridge University Press.

Wrangham RW. 2009. *Catching Fire. How Cooking Made Us Human*. London: Profile Books LTD.

Yizhaq M, Mintz G, Cohen I, Khalaily H, Weiner S, Boaretto E. 2005. Quality controlled radiocarbon dating of bones and charcoal from the early Pre-Pottery Neolitic B (PPNB) of Motza (Israel). *Radiocarbon* 47(2):193–206.